Effect of Strut Geometric Imperfections on the Internal Forces Distribution in Tensegrity Structures

Basile Payen[1], Pierre Latteur[2], and João Pacheco de Almeida[3]

[1]Ph.D. candidate, UCLouvain, Institute of Mechanics, Materials and Civil Engineering, Civil and Environmental Engineering, Place du Levant, 1 (Vinci), bte L5.05.01, Louvain-la-Neuve 1348, Belgium. ORCID: https://orcid.org/0009-0000-6763-1411. Email: basile.payen@uclouvain.be (Corresponding author)

[2]Professor, UCLouvain, Institute of Mechanics, Materials and Civil Engineering, Civil and Environmental Engineering, Place du Levant, 1 (Vinci), bte L5.05.01, Louvain-la-Neuve 1348, Belgium. ORCID: https://orcid.org/0000-0002-4608-3732. Email: pierre.latteur@uclouvain.be

[3]Assistant Professor, UCLouvain, Institute of Mechanics, Materials and Civil Engineering, Civil and Environmental Engineering, Place du Levant, 1 (Vinci), bte L5.05.01, Louvain-la-Neuve 1348, Belgium. ORCID: https://orcid.org/0000-0001-6299-6593. Email: joao.almeida@uclouvain.be

This is an Accepted Manuscript of an article published by ASCE in the Journal of Structural Engineering on Feb 25, 2026, available online: https://doi.org/10.1061/JSENDH.STENG-15452

References for the article:
Payen B., Latteur P., Almeida J., 2026, "Effect of Strut Geometric Imperfections on the Internal Forces Distribution in Tensegrity Structures", **Journal of Structural Engineering**, *152* (5) DOI: 10.1061/JSENDH.STENG-15452

ABSTRACT
Tensegrity structures are valued for their distinctive look, deployability, and potential for active control, making them attractive candidates for applications in civil engineering, architectural, and space structures. Recent large-scale experiments have revealed discrepancies with numerical model simulations when significant external loads or prestress are applied. These differences can be due to initial geometric imperfections of compressed struts, which lead to an elastic bending causing a reduction in the struts' axial stiffness. This affects the distribution of prestress and internal forces, as well as the structural stiffness and load-bearing capacity. This article focuses on the influence of the out-of-straightness of struts on the distribution of prestress and internal forces, and how these geometric imperfections should be considered to obtain more reliable models for design and assessment. The first part of this work develops a dimensionless analytical expression for the loss of strut stiffness due to out-of-straightness. The second part explains how this analytical expression can be integrated into a numerical code developed by the authors, called Muscle, for calculating tensegrity structures. In the third part, the approach is validated on two previously tested prototypes, an aluminum simplex and a 15 m bamboo footbridge, demonstrating that geometric imperfections can change internal forces by tens of percent. The proposed formulation thus provides a computationally efficient and general framework for incorporating imperfection-induced stiffness reduction into the analysis and design of tensegrity structures.

KEYWORDS: Tensegrity structures, Initial geometric imperfection, Strut out-of-straightness, Nonlinear analysis, Axial stiffness, Elastic bending, Flexural buckling, Dynamic relaxation.

PRACTICAL APPLICATIONS

Tensegrity has been discussed by engineers and architects for decades. However, the number of tensegrity structures built as part of civil engineering and architectural projects is extremely limited worldwide. There are several reasons for this, including the lack of confidence engineers have in these complex structures, which in turn is due to a lack of confidence in the programs used to calculate and design them. This investigation deals with geometric imperfections in struts, which many consider negligible, but which in reality is shown to have a major impact on the value and distribution of internal forces. This article explains how this phenomenon was integrated into the open-source Grasshopper plug-in Muscle, which was developed by the authors for the calculation and design of tensegrity structures. This article will therefore enable Muscle users to calculate tensegrity structures with high reliability and to design them according to the required safety standards.

INTRODUCTION

Tensegrity structures are composed of struts in a set of tensioned cables (Motro 2003). They are studied across various fields: metamaterials, space applications, architecture, and civil engineering (Micheletti and Podio-Guidugli 2022). Tensegrity is synonym with visually striking architecture, active structures, and deployability, with ongoing research focusing on large-scale applications (Rhode-Barbarigos et al. 2012; Shekastehband et al. 2013; Feron et al. 2019). Lightweight design is also often cited as an advantage, however, this is not always accurate, as the need for prestress to ensure adequate stiffness can increase the structural weight (Latteur et al. 2017).

Numerical methods based on form-finding, such as dynamic relaxation (Barnes 1999; Bel Hadj Ali et al. 2011) and the force density method (Zhang and Ohsaki 2006) are commonly used to model the geometrically nonlinear and prestressed behavior of tensegrity structures. They are mainly based on the assumption of a prestressed truss-like structure, with pin-jointed nodes, subjected to external forces, transmitting only axial forces (compression in struts and tension in cables), and linear-elastic materials.

In real conditions however, initial geometrical imperfections in the struts, arising from the manufacturing processes of metal struts, the irregular nature of timber if used as logs or bamboo struts, or other sources of imperfection associated with other materials, result in a reduction of their effective axial stiffness, and in the appearance of parasitic bending moments. This phenomenon, which marks the preliminary stage of buckling, subsequently leads to a redistribution of prestress and internal forces, which has been highlighted by the authors when comparing experimental results with numerical ones (Feron et al. 2023).

Buckling was largely documented since the 1960s, with, among others, key studies about the buckling curves for metals (Maquoi and Rondal 1978) on which are based the current European standards (CEN 2005, 2007). Recent studies have examined the flexural buckling behavior of compressed steel member based on geometrically and materially nonlinear analyses with imperfections (Jeppe Jönsson et al. 2017; Saufnay et al. 2024).

Geometrical imperfections cause the struts to experience a combination of bending and compression, rather than pure compression as assumed in ideal truss models (Cai et al. 2018). Experiments on a 2-meter aluminum simplex showed up to 10 % discrepancy in the internal forces between dynamic relaxation models and experimental results (Feron et al. 2023). Other tests comparing a simplex with slender struts to one with stockier members (Rutkiewicz and Małyszko 2024) showed significantly different behaviors due to elastic bending in the slender bars-an effect consistently neglected in current truss-based models (Cai et al. 2019; Feron et al. 2024).

Numerical models using modified dynamic relaxation (Barnes et al. 2013) can include imperfections in the struts but at the cost of increased complexity and longer computation times, making them less suitable for large-scale applications. Complementary developments have focused on improving the overall efficiency and stability of tensegrity systems, for instance through topology optimization considering buckling constraints (Xu et al. 2018) or form-finding based on rank minimization of the force-density matrix (Wang et al. 2021). An alternative approach is to use a stiffness reduction method that links the axial stiffness of a perfectly straight element to one with imperfections (Kucukler et al. 2014), typically on design codes (e.g., Eurocode) and valid for a single imperfect shape; this paper extends such approaches by providing a continuous stiffness-load relationship describing the progressive degradation of imperfect struts during both prestressing and external loading phases.

The present article addresses the research gap identified above and starts with developing a unique analytical formulation for the imperfection-induced axial stiffness reduction of struts. Independent of design codes, it relies solely on parameters already used for numerical modeling. The formulation can be easily integrated into existing truss-based numerical codes without significantly affecting computational efficiency. This analytical formulation is then numerically validated and incorporated into the dynamic relaxation process within the open-source Rhino-Grasshopper (McNeel 2025) plug-in Muscle developed by the authors (Feron et al. 2024). The last part of the article concerns two large-scale prototypes built and tested by the authors, for which internal forces were computed using the modified Muscle numerical code, considering various assumptions of strut geometric imperfections.

ANALYTICAL AXIAL STIFFNESS MODEL FOR A GEOMETRICALLY IMPERFECT STRUT

This section develops the analytical formulation of the equivalent axial stiffness for a geometrically imperfect strut (Fig. 1), which will be expressed as a function of the axial load ratio and geometric dimensionless parameters. An expression for the first yield axial load ratio is also derived. The model is then validated using nonlinear finite element software and evaluated in light of the buckling criteria defined in European standards. The influence of the shape of the initial imperfection is also addressed.

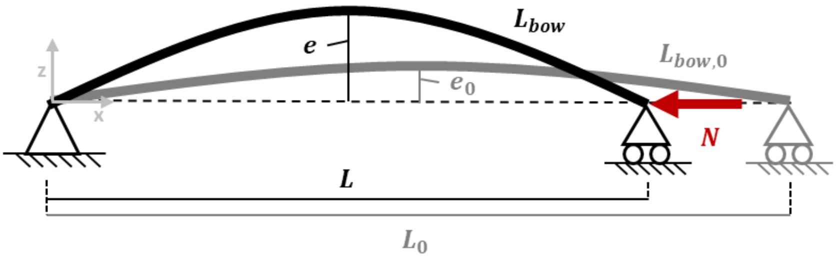

Fig. 1. Geometrically imperfect strut under axial loading, resulting in elastic bending.

Analytical expression for the equivalent stiffness reduction

Consider the strut in Fig. 1, where L_0 denotes the length of the chord between the supports in the initial (undeformed) configuration. The strut has a cross-section area A, Young's modulus E, and is compressed by an axial force N. The following expressions are considered for the strut's axial stiffness:

- $K = EA/L_0$, the stiffness of the strut considered as perfectly straight, i.e. without initial geometric imperfection.
- $K_{red} = \mathrm{N}/(L_0 - L)$, the reduced equivalent stiffness of the geometrically imperfect strut, which depends directly on the axial load N and indirectly through the nonlinear dependence of L on N; the term 'equivalent' is used to indicate that the stiffness is measured along the strut's chord direction.

In this article, their ratio as defined below is called the *stiffness reduction factor*:

$$\frac{K_{red}}{K} = \frac{N}{EA}\left(1 - \frac{L}{L_0}\right)^{-1} \leq 1 \qquad (1)$$

The following developments focus on deriving the analytical expression for the factor L/L_0.

The initial transverse profile of the geometrically imperfect strut axis is assumed to follow Eq. (2), which represents a half-period sinusoidal function with amplitude e_0 that is commonly used to model initial imperfections (Somodi et al. 2023; Saufnay et al. 2024):

$$z_0(x) = e_0 \sin\left(\pi \frac{x}{L_0}\right) \qquad (2)$$

The expression for the deflected shape after the application of the axial load is also assumed to be sinusoidal and includes the second order amplification factor $(1 - N/N_{cr})^{-1}$, where $N_{cr} = \pi^2 EI/L_0^2$ is the buckling load:

$$z(x) = e \sin\left(\pi \frac{x}{L}\right) = e_0 \left(1 - \frac{N}{N_{cr}}\right)^{-1} \sin\left(\pi \frac{x}{L}\right) \tag{3}$$

With

$$e = e_0 \left(1 - \frac{N}{N_{cr}}\right)^{-1} \tag{4}$$

If $L_{bow,0}$ and L_{bow} are, respectively, the bow length of the deformed strut before and after application of the axial load, they can be calculated as follows, assuming $\sqrt{1+\epsilon} \approx 1 + \frac{\epsilon}{2} + \cdots$ (considering $\epsilon \ll 1$):

$$L_{bow,0} = \int_0^{L_0} \sqrt{1 + \pi^2 \left(\frac{e_0}{L_0}\right)^2 \cos^2\left(\pi \frac{x}{L_0}\right)}\, dx \approx L_0 \left(1 + \frac{\pi^2}{4}\left(\frac{e_0}{L_0}\right)^2\right) \tag{5}$$

$$L_{bow} \approx L \left(1 + \frac{\pi^2}{4}\left(\frac{e}{L}\right)^2\right) \tag{6}$$

The difference between $L_{bow,0}$ and L_{bow} is due to the elastic shortening induced by the axial load:

$$L_{bow} = L_{bow,0} - \frac{N L_{bow,0}}{EA} \tag{7}$$

Since $e_0 \ll L_0$, Eq. (5) simplifies to $L_{bow,0} \approx L_0$. Introducing this and Eq. (6) into Eq. (7) leads to:

$$\frac{L}{L_0}\left(1 + \frac{\pi^2}{4}\left(\frac{e}{L}\right)^2\right) = 1 - \frac{N}{EA} \tag{8}$$

The second term on the right-hand side can be expressed using the slenderness ratio $\lambda = L_0\sqrt{A/I}$:

$$\frac{N}{EA} = \frac{N}{N_{cr}}\frac{N_{cr}}{EA} = \pi^2 \frac{1}{\lambda^2}\frac{N}{N_{cr}} \tag{9}$$

Introducing in Eq. (8), additionally, the relation between the amplitude in the deformed and initial configurations of Eq. (4), leads to a quadratic form whose positive root is given by the following expression:

$$\begin{aligned}\frac{L}{L_0} &= 0.5 + \frac{\pi^2}{8}\left(\frac{e_0}{L_0}\right)^2 - \frac{\pi^2}{2}\frac{N}{N_{cr}}\frac{1}{\lambda^2} + \sqrt{\left(0.5 + \frac{\pi^2}{8}\left(\frac{e_0}{L_0}\right)^2 - \frac{\pi^2}{2}\frac{N}{N_{cr}}\frac{1}{\lambda^2}\right)^2 - \frac{\pi^2}{4}\left(\frac{e_0}{L_0}\right)^2 \frac{1}{(1 - N/N_{cr})^2}} \\ &= function\left(\frac{N}{N_{cr}}, \frac{e_0}{L_0}, \lambda\right)\end{aligned} \tag{10}$$

Eq. (10), which is expressed in terms of dimensionless parameters, can be introduced in Eq. (1), together with Eq. (9), to obtain the following expression for the stiffness reduction factor K_{red}/K:

$$\frac{K_{red}}{K} = \pi^2 \frac{1}{\lambda^2}\frac{N}{N_{cr}}\left(1 - \frac{L}{L_0}\right)^{-1} = function\left(\frac{N}{N_{cr}}, \frac{e_0}{L_0}, \lambda\right) \leq 1 \tag{11}$$

K_{red}/K, which characterizes the loss of axial rigidity induced by the initial geometrical imperfection, has thus an explicit analytical expression that depends only on 3 dimensionless parameters: the axial load ratio N/N_{cr}, the imperfection amplitude ratio e_0/L_0, and the strut slenderness ratio λ.

Analytical expression for the first yield axial load

Determining the axial force N_{max} at which first yielding occurs is also important, and can be obtained as follows, where W_{el} is the elastic section modulus:

$$\frac{N_{max}}{A} + \frac{\left(1 - \frac{N_{max}}{N_{cr}}\right)^{-1} e_0 \, N_{max}}{W_{el}} = f_y \tag{12}$$

Eq. (12) can be reformulated to obtain:

$$\frac{N_{max}}{N_{cr}} \frac{N_{cr}}{A f_y} + \left(1 - \frac{N_{max}}{N_{cr}}\right)^{-1} \frac{N_{max}}{N_{cr}} \frac{N_{cr}}{A f_y} \frac{A e_0}{W_{el}} = 1 \tag{13}$$

If the relative slenderness ratio is defined as $\lambda_{rel} = \sqrt{A f_y / N_{cr}}$, Eq. (13) leads to:

$$\frac{N_{max}}{N_{cr}} = 0.5\left(1 + {\lambda_{rel}}^2 + \frac{A e_0}{W_{el}} + \sqrt{\left(1 + {\lambda_{rel}}^2 + \frac{A e_0}{W_{el}}\right)^2 - 4{\lambda_{rel}}^2}\right) = function\left(\frac{A e_0}{W_{el}}, \lambda_{rel}\right) \tag{14}$$

Eqs. (14) and (11) define the maximum axial load above which the bending leads to a stress higher than f_y, and the stiffness reduction factor, respectively. These analytical relations were implemented in Muscle to quantify the effect of geometrical imperfections on prestress loss, internal forces, and overall stiffness of tensegrity structures, as discussed in the next sections.

Influence of initial imperfection e_0/L_0 on K_{red} and validation of analytical expressions

The previous developments are examined through the example of an aluminum strut ($E = 70{,}390$ MPa, $f_y = 160$ MPa) with a hollow circular cross-section (outside diameter 60 mm, thickness 2 mm) and slenderness ratio $\lambda = 146.2$. Such strut is similar to the ones used in the tensegrity prototype tested by Feron et al. (2023) and employed in a case study later in this article. Some relevant reference values of the axial load are:

- Plastic axial force capacity, i.e. neglecting buckling: $f_y * A = 58.3$ kN.
- Euler buckling load: $N_{cr} = 11.8$ kN (which implies a relative slenderness ratio of $\lambda_{rel} = 2.2$).
- Axial buckling load according to EC9 (CEN 2007): $N_{EC9} = 10.7$ kN.
- Axial load at first yielding with $e_0/L_0 = 1/300$ using Eq. (14): $N_{\max} = 10.0$ kN.

Fig. 2 compares, for different values of initial imperfection e_0/L_0, the values of the ratio K_{red}/K for the aluminum strut obtained according to four different methods:

- Analytical expression of Eq. (11).
- Eurocode 9 (CEN 2007) with buckling curve A: the Eurocode model assumes a strut with “full” axial stiffness $K = EA/L$ up to the onset of buckling, which occurs when the axial force reaches $N_{EC9} = 10.66$ kN. This assumption is commonly adopted in many current models.
- Numerical simulations with second-order nonlinear finite elements with linear elastic material, using Karamba3D (Preisinger 2013).
- Numerical simulations with geometrically nonlinear finite elements (namely, through beam corotational formulation) with elastic-perfectly plastic material (yield strength $f_y = 160$ MPa, as indicated above), using Seismostruct (Seismosoft 2024).

Both numerical simulations employed a discretization of the strut into 60 beam elements, determined to be sufficient for mesh-independent results while allowing precise initial imperfection shapes.

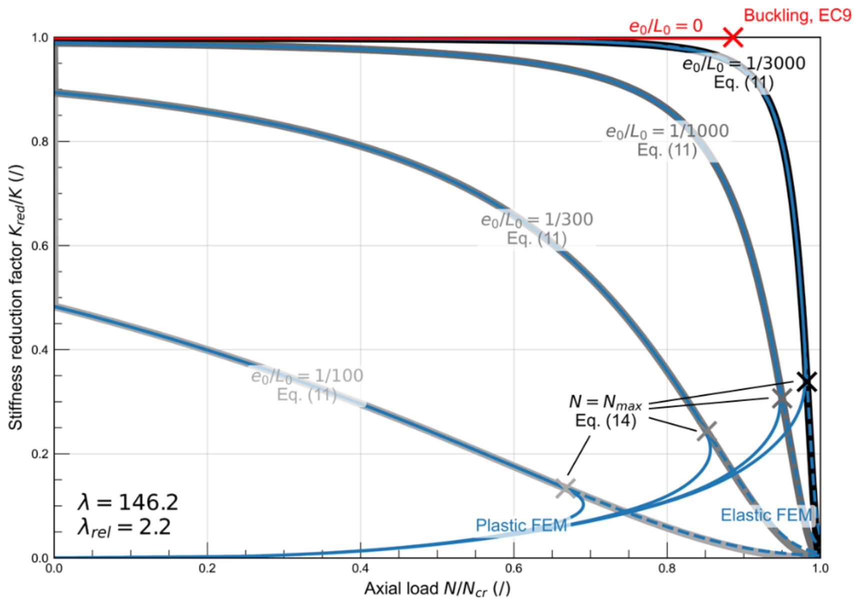

Fig. 2. Variation of the stiffness reduction factor computed for an aluminum strut using four different methods and various initial imperfection amplitudes.

Eq. (14) also allows calculating the value of the axial force N_{max} at first yielding, shown with crosses in Fig. 2, which is not covered by the Eurocode.

Fig. 2 shows:

- The analytical formulation (Eq. (11)) shows very good accuracy in estimating the stiffness reduction factor. The curves from Eq. (11) closely match the numerical results up to $N = N_{max}$, thereby validating the analytical expression.
- The progressive decrease of the axial stiffness, which becomes nonlinearly more pronounced as N/N_{cr} increases.
- A strong sensitivity of the stiffness reduction factor K_{red}/K to the initial imperfection amplitude e_0/L_0.
- Eq. (14) provides a good estimation of the onset of yielding in the strut, corresponding to the point where the plastic FEM response starts to deviate from the elastic response. This also indicates that Eq. (11) is no longer valid beyond N_{max}. It is noted that truss structures are designed to remain elastic.
- The discrepancy between the response of geometrically perfect and imperfect struts is non-negligible, which strengthens the need to consider realistic axial stiffness that depends on the value of the axial force and its interplay with geometric imperfections.

Influence of the shape of the initial imperfection on K_{red}

The results presented above, along with Eqs. (11) and (14), are based on the assumption of an initial sinusoidal imperfection shape, which may not accurately represent realistic conditions. To evaluate the impact of this assumption, seven alternative imperfection shapes are herein analyzed, as illustrated in Fig. 3. For each shape, the stiffness reduction factor K_{red}/K was computed using a second-order nonlinear finite element analysis with an elastic material model in Karamba3D (Preisinger 2013), the results of which are presented in Fig. 4. The considered shapes are:

- The reference shape: half sine wave shown in Fig. 1.
- Fig. 3(a and b): sine waves with shorter wavelength.
- Fig. 3(c): bilinear profile.
- Fig. 3(d, e and f): localized imperfection shapes with varying lengths.

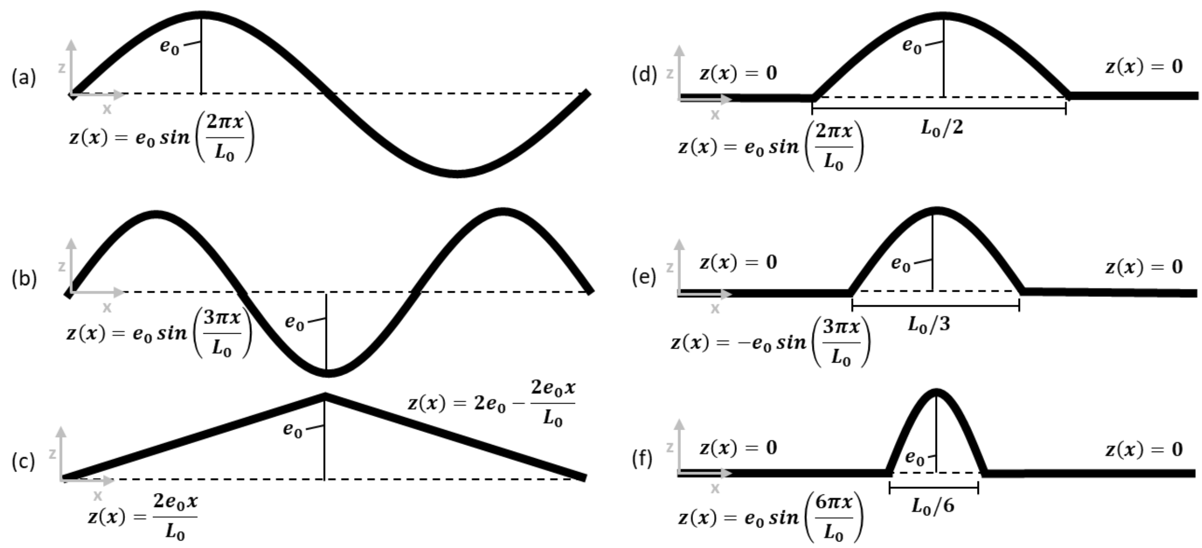

Fig. 3. Different initial imperfection shapes considered: (a) full sine, (b) 1.5 sine periods, (c) bilinear shape, variation of imperfection width with (d) half-length, (e) one-third, and (f) one-sixth of the total length.

Fig. 4(a) highlights the influence of imperfection shape on the stiffness reduction factor K_{red}/K, while Fig. 4(b) illustrates the effect of the imperfection length. The strut's geometrical and material properties are identical to those used previously, with an initial imperfection amplitude of $e_0/L_0 = 1/300$.

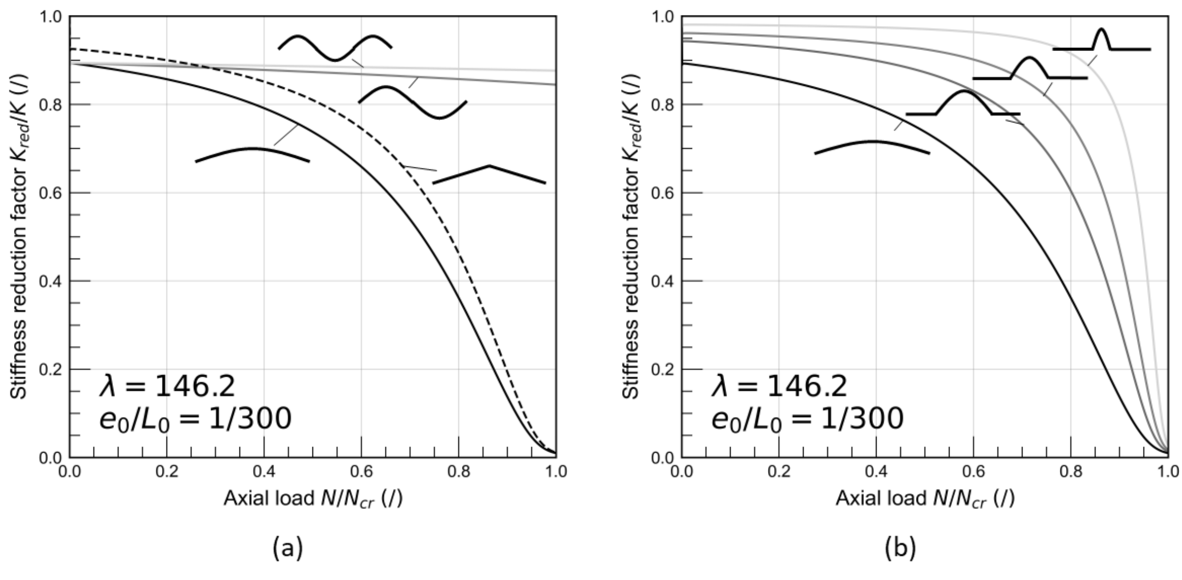

Fig. 4. Variation of the stiffness reduction factor for different (a) shapes and (b) lengths of initial imperfections.

Fig. 4 shows:

- The significant impact of both the shape and length of the initial imperfection on the equivalent axial stiffness of the strut.
- That the previously considered half sine wave imperfection is the most conservative case, as it leads to the greatest stiffness reduction.

The half sine wave is seen to represent the most conservative imperfection case for structural design, at least when serviceability deformation limit states are considered. Moreover, it is believed to be one common imperfection in practice, and it enables the use of simplified analytical expressions, avoiding the need for finite element simulations. While the actual imperfection shape of a strut depends on the material, cross-section, and other factors, the method can accommodate alternative shapes, which can be implemented on a project-specific basis; in this paper, the half-sine shape is employed along with Eq. (11) validated in the previous subsection, enabling direct integration of the equivalent axial stiffness reduction factor into numerical models, as detailed in the next section.

MODIFICATION OF THE DYNAMIC RELAXATION NUMERICAL CODE OF MUSCLE

The analytically-derived stiffness reduction expression (Eq. (11)) has been integrated into Muscle's numerical code (Fig. 5), an open-source Grasshopper plug-in developed by Feron et al. (2024). Both the plug-in and the numerical calculation codes are freely available on GitHub (Feron 2025).

Muscle employs a truss-like finite element model to identify mechanisms and self-stress modes of tensegrity structures through Singular Value Decomposition (Pellegrino 1993). It also enables their form-finding, the simulation of deployments, and nonlinear structural analysis using the dynamic relaxation (DR) method (Barnes 1999; Bel Hadj Ali et al. 2011), all of them through the parametric environment of Rhino-Grasshopper (McNeel 2025).

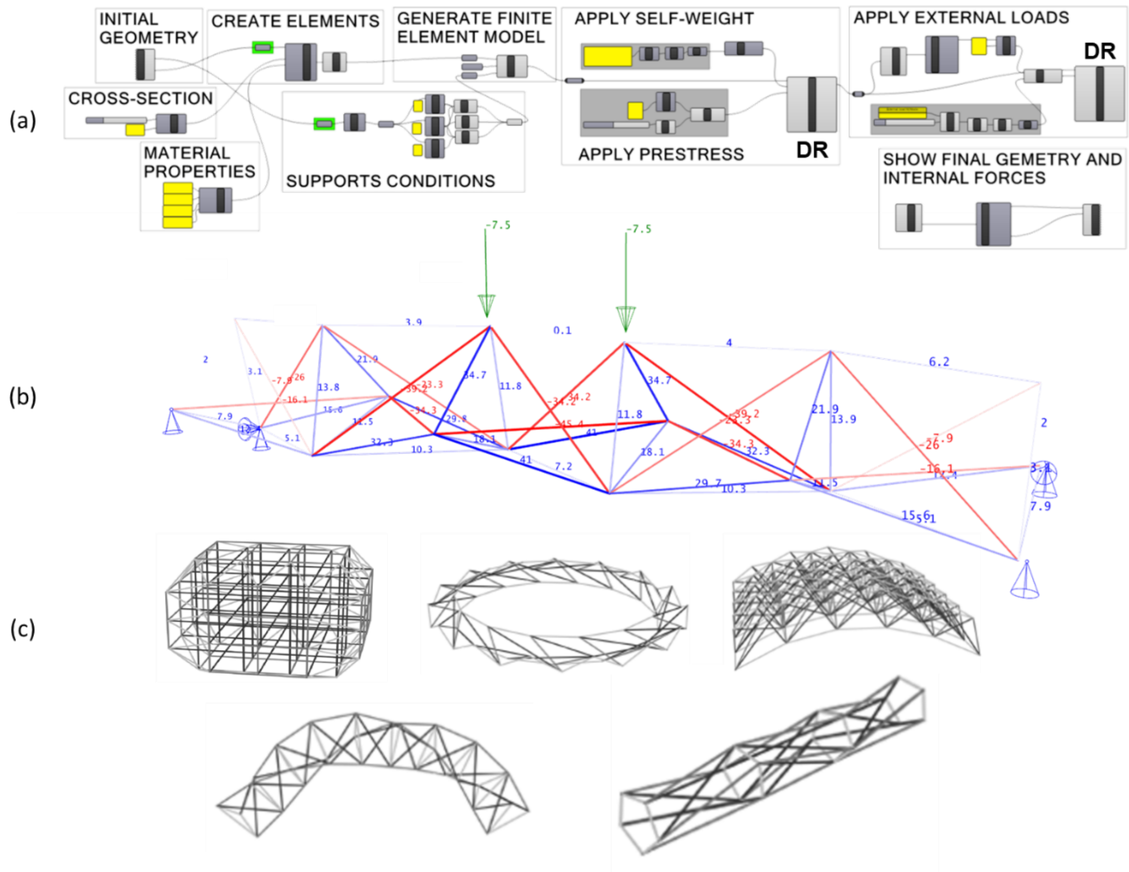

Fig. 5. (a) Muscle user interface in Grasshopper, illustrating model generation, load application, and dynamic relaxation. (b) Result shown with final deformed shape and internal forces with one of the case studies described further in this article (red: compression, blue: tension). (c) Other families of tensegrity structures that can be designed and calculated by Muscle.

The existing model algorithm in Muscle considering perfectly straight struts is presented by the dashed boxes in Fig. 6: after defining the input properties (1), the DR method is executed (2) to compute the final geometry (11). The implementation of the model in Grasshopper is shown in Fig. 5(a). In other words, the available DR implementation in Muscle assumes constant axial stiffness and does not account for reductions due to initial imperfections in the struts.

By incorporating the expression of Eq. (11) while keeping the truss model, the simulation can directly include the decrease of the equivalent axial stiffness arising from geometric imperfections. Fig. 6 outlines the updated algorithm of the numerical code including the new processes and decision boxes with solid contour lines. Following the definition of the initial geometry of the structure, including initial length (L_0), cross-sections, supports, prestress levels (Feron and Latteur 2023), and position and values of external loads (1), a first DR iteration is performed to compute internal forces and nodal displacements (2). Based on the latter and a defined initial imperfection amplitude (3), the stiffness reduction factor K_{red}/K is computed (4) for each strut with Eq. (11) and applied by scaling its Young's modulus (for computational convenience; it results in an equivalent strut stiffness correction).

Since the stiffness reduction depends on the estimated internal axial force, which itself is influenced by the strut stiffness, an iterative approach is required. This was implemented through the following loop:

- (5) The dynamic relaxation (DR) method is executed.
- (6) If the change of axial force in any strut with respect to the previous iteration, $|N_{\mathrm{i}} - N_{\mathrm{i-1}}|$, exceeds the prescribed tolerance, the loop continues.
- (7) The stiffness reduction factor is updated using Eq. (11).
- (8) A bisection algorithm is applied to exploit the monotonic relationship between axial force and stiffness, ensuring unconditionally stable and efficient convergence with fewer DR iterations.

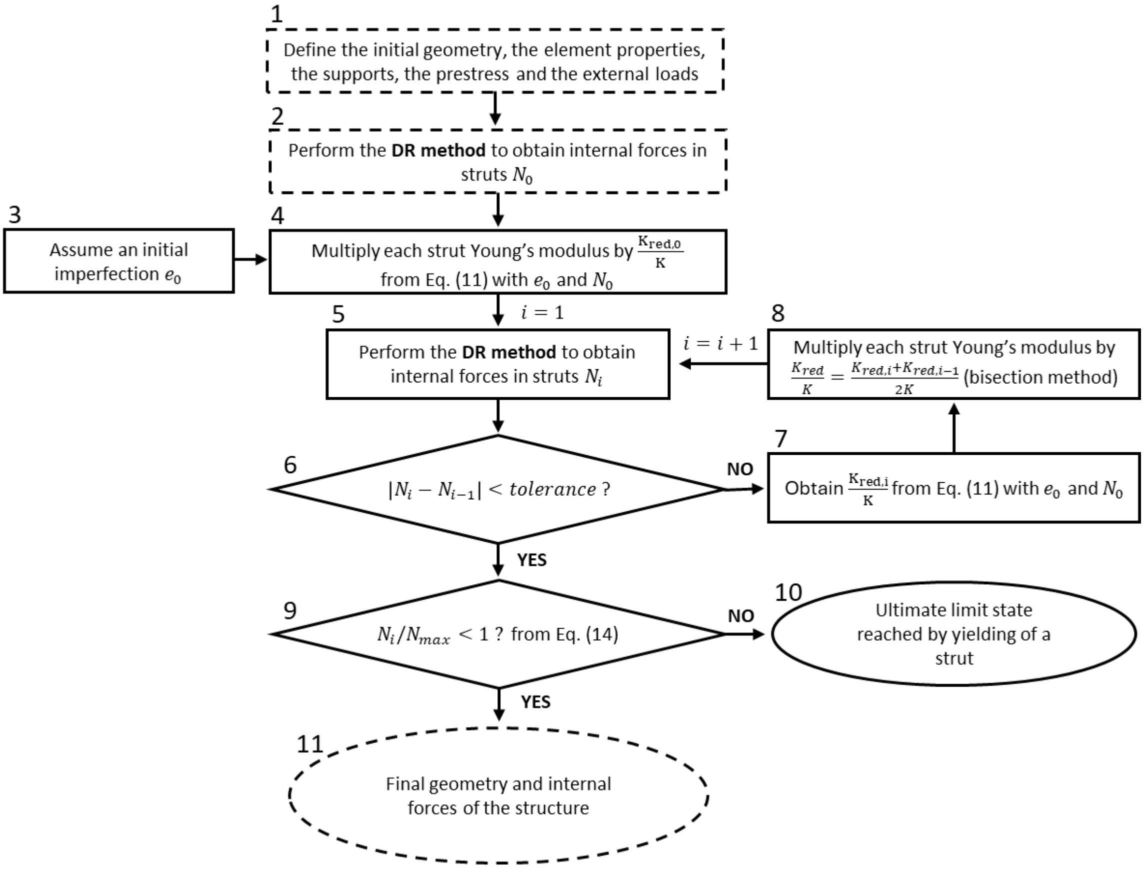

Fig. 6. General computational algorithm in Muscle: the dashed boxes correspond to the perfectly straight strut model previously implemented, whereas the processes and decision nodes with solid contour lines are new adaptations to consider the effect of initial geometric imperfections.

Once the tolerance is met, two outcomes are possible (9):

- (10) If any strut force exceeds the first yield limit N_{max}, the elastic assumption is no longer valid, and the structure is considered to have reached its ultimate limit state.
- (11) Otherwise, the equilibrium configuration and internal forces are obtained.

With the above modifications, the updated version of Muscle was used in the following two case studies to illustrate the impact of struts' initial imperfections on the internal force distribution of structures. Despite the additional iterations, a complete analysis in Grasshopper considering imperfections requires approximately 0.5 s for simple structures and up to 5 s for more complex ones, compared to about 0.1 s to 0.5 s for a standard dynamic relaxation calculation without imperfections, which remains fully acceptable for computational analyses and potential optimization loops.

APPLICATION TO TENSEGRITY STRUCTURES

This section illustrates and quantifies the impact of initial imperfections on the behavior of tensegrity structures. The first case study is an aluminum simplex (Feron et al. 2023), while the second is a 15-meter-span bamboo structure (Feron and Latteur 2023; Labrouche and Houriez 2023).

Basic aluminum simplex

The simplex structure built and tested at UCLouvain (Feron et al. 2023) is composed of three aluminum struts and nine aluminum cables, with three external loads applied at the top nodes. The experimental setup is shown in Fig. 7(a). The geometry illustrated in Fig. 7(b) corresponds to an initial condition with no external loads but with prestress resulting in 1.5 kN compression in the struts, 0.98 kN tension in the vertically oblique cables, and 0.59 kN tension in the horizontal cables. The simplex has a height of $1{,}950$ mm, circumscribed circle diameter of $2{,}360$ mm for the equilateral bottom and top horizontal triangular bases, and a $30°$ rotation between the two bases. The structure was then subjected to three loads applied downwards on each top node, ranging from 0 kN to 2.1 kN.

The mechanical properties of the struts and cables were determined through experimental characterization tests for the Young's modulus E, and provided by the supplier for the yield strength f_y. These values, along with the geometrical properties of the struts, are summarized in Table 1. They provide $\lambda = 146.2$, $\lambda_{rel} = 2.2$, $f_y * A = $ 58.3 kN, $N_{cr} = 11.8$ kN, $N_{EC9} = 10.7$ kN (EC9), and $N_{\max} = 10.0$ kN from Eq. (14) with $e_0/L_0 = 1/300$.

Table 1. Element properties of the aluminum simplex.

Elements	E (MPa)	f_y (MPa)	Diameter (mm)	Thickness (mm)	L_0 (mm)
Strut	70390	160	60	2	2999.8
Vertical cables	72190	120	8	/	2043.4
Horizontal cables	71750	120	8	/	2043.8

The struts and the cables were fitted with elongation devices or turnbuckles in order to set the prestress and their stiffness is considered with an equivalent Young's modulus. All element characterization tests and experimental results are openly accessible (Feron et al. 2022). Node 1 is blocked in x, y and z directions, node 0 is fixed along the y and z directions, and node 2 is only blocked in the vertical z direction.

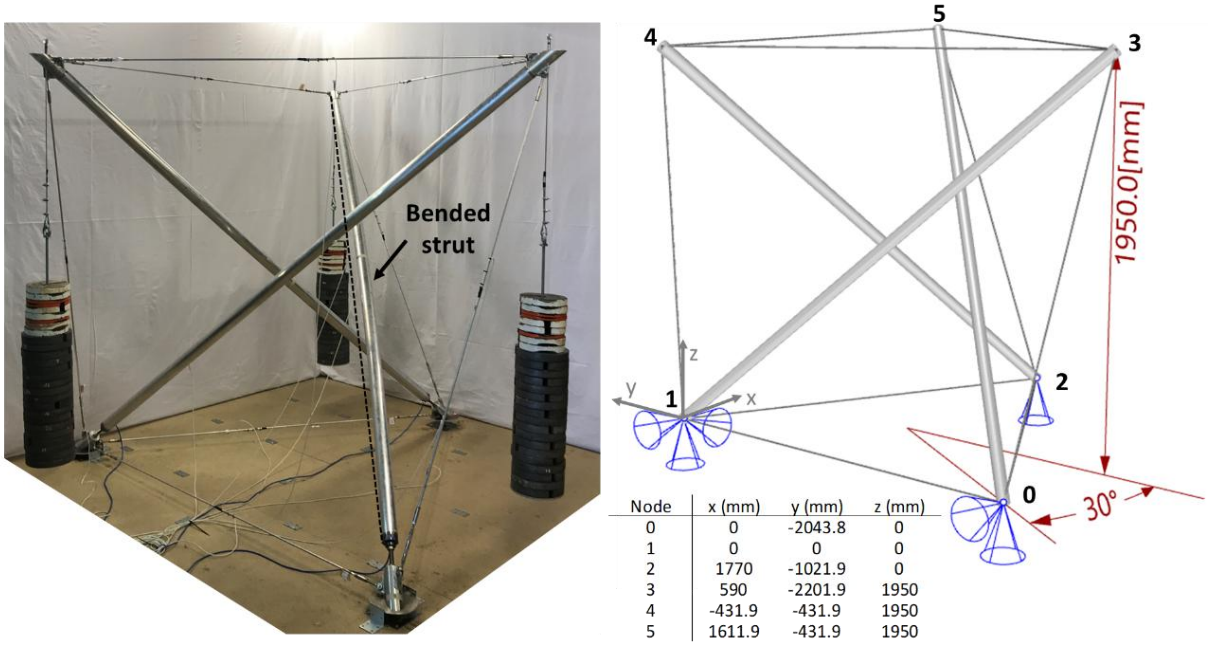

Node	x (mm)	y (mm)	z (mm)
0	0	-2043.8	0
1	0	0	0
2	1770	-1021.9	0
3	590	-2201.9	1950
4	-431.9	-431.9	1950
5	1611.9	-431.9	1950

(a) (b)

Fig. 7. Aluminum simplex tested at UCLouvain: (a) experimental campaign setup (image by authors) and (b) node coordinates and dimensions.

Fig. 8(a) shows, for increasing values of the external loads, the internal forces measured in the three struts and in the horizontal cables. The strut bending observed during testing is clearly visible in Fig. 7(a). The values of the internal forces computed numerically with Muscle are also depicted, which include the analytical expression of the reduction stiffness coefficient. Four levels of imperfection were considered: $e_0/L_0 = 0$, $e_0/\mathrm{L}_0 = 1/1000$ (which corresponds approximately to the measured geometric imperfection of the employed aluminum struts), $e_0/\mathrm{L}_0 = 1/300$ (recommended by Eurocode 9 (CEN 2007)), and $e_0/\mathrm{L}_0 = 1/100$ (highly imperfect strut, which can also simulate a damaged member).

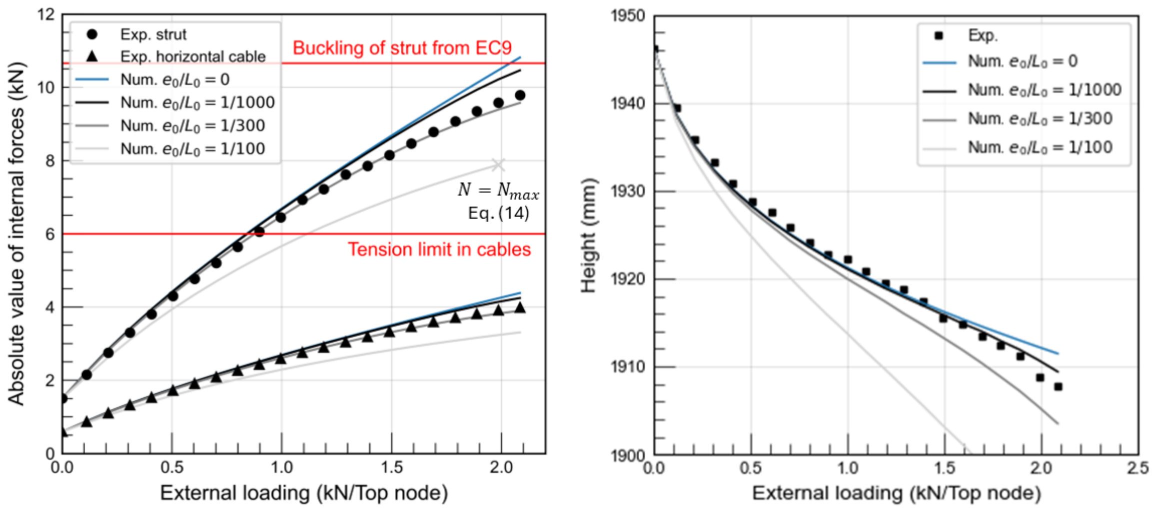

(a) (b)

Fig. 8. Comparison between experimental results and Muscle model of the aluminum simplex, for different initial strut imperfection amplitudes, under increasing external loading: (a) internal forces in the struts and horizontal cables, and (b) evolution of the simplex height.

Fig. 8(a) shows that:

- The numerical model without imperfections ($e_0/L_0 = 0$, top blue curve) fails to capture the experimental behavior at higher external loads, leading to an overestimation of the strut and cable internal forces by about 10%.
- The numerical model with $e_0/L_0 = 1/300$ (as recommended by Eurocode 9) provides a better fit with the experimental results, showing a relative error of up to 2.2% in the strut internal force. Although this may seem counterintuitive, given that the measured average imperfection of the struts was $e_0/L_0 = 1/1000$, the $e_0/L_0 = 1/300$ assumption adopted by the Eurocode accounts not only for geometric imperfections but also for other effects, such as residual stresses, which also induce elastic bending.
- The initial imperfection of $e_0/L_0 = 1/100$ is intentionally exaggerated but serves to illustrate how significant strut imperfections can substantially affect internal forces—up to 20% increase in strut forces—along with premature yielding due to bending stresses (indicated by the small gray cross in Fig. 8(a)).

Fig. 8(b) shows the evolution of the simplex structure's height, which captures its global deflection. The model with $e_0/L_0 = 1/1000$ better matches the experimental results than the $e_0/L_0 = 1/300$ case, highlighting the need for a realistic estimate of e_0/L_0, ideally informed by experimental data, while remaining differences may arise from model assumptions or experimental uncertainties.

For this simple structure, the results demonstrate the influence of initial imperfections on the internal forces within the structural elements. The proposed method successfully captures strut bending and provides a closer match to the experimental results. The next section extends the analysis to a more complex and realistic structure to further analyze the redistribution of prestress.

Bamboo structure

A bamboo structure (Fig. 9) was designed, built, and tested at UCLouvain (UCLouvain GCE 2023; Feron and Latteur 2023; Labrouche and Houriez 2023). Inspired by the "Snake Bridge" (Feron et al. 2019; UCLouvain GCE 2020) , the structure is composed of five simplex modules made of bamboo struts and steel cables, with an overall span of 14.7 m and a total self-weight of 624 kg.

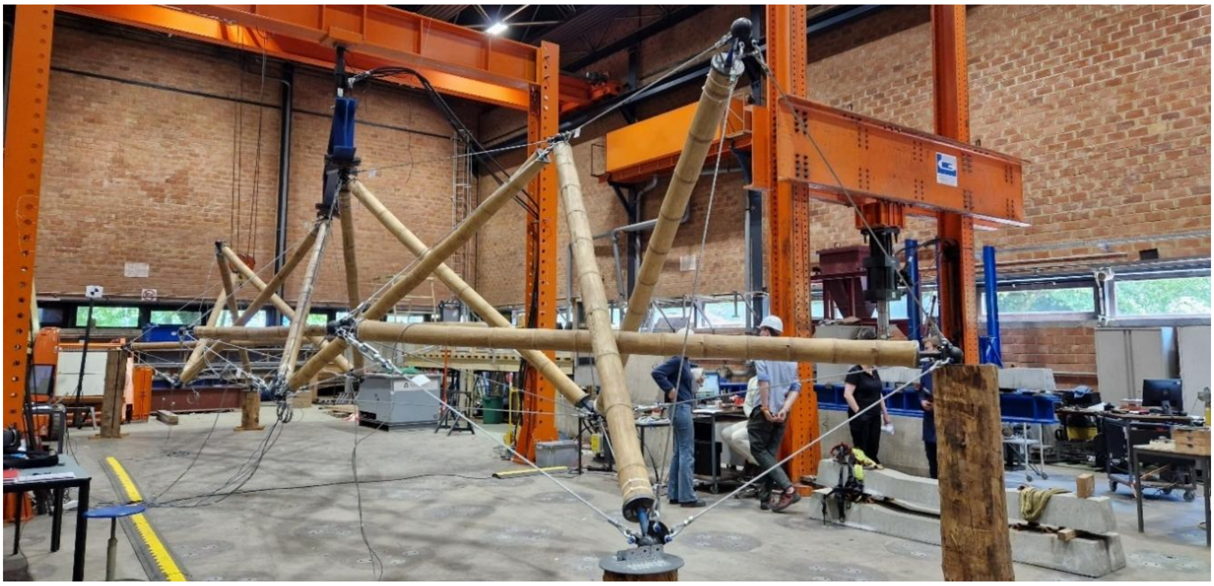

Fig. 9. Global view of the bamboo tensegrity structure in the LEMSC laboratory, at UCLouvain, Belgium (image by authors).

A detailed view of the structure and node numbering is shown in Fig. 10. Struts are labelled with a “S” and cables with a “C”, followed by the indices of the nodes they connect (e.g., S2-8, C3-7). One additional diagonal cable was added to each module to block mechanisms and enhance global stiffness (C2-3, C3-8, C8-9, C9-14 and C14-15). The bottom longitudinal cables, such as C0–3 and C2–5 for Module 1, were equipped with turnbuckles to enable the application of adjustable prestress. The supports block the vertical displacement of node 15 in the *z* direction, node 17 in the *y* and *z* directions, and node 2 along the three directions (Fig. 10). The mechanical and geometrical properties were obtained from experimental characterization (e.g., the Young’s modulus E) or from the supplier’s specifications (e.g., the yield strength f_y, which for the struts is taken as a limit of elasticity along the bamboo strut longitudinal axis) and are reported in Table 2. For the struts, the following parameters are obtained: $\lambda = 84.9$, $\lambda_{rel} = 3.02$, $f_y * A = 459.5$ kN, $N_{cr} = 50.3$ kN and $N_{\max} = 47.3$ kN from Eq. (14).

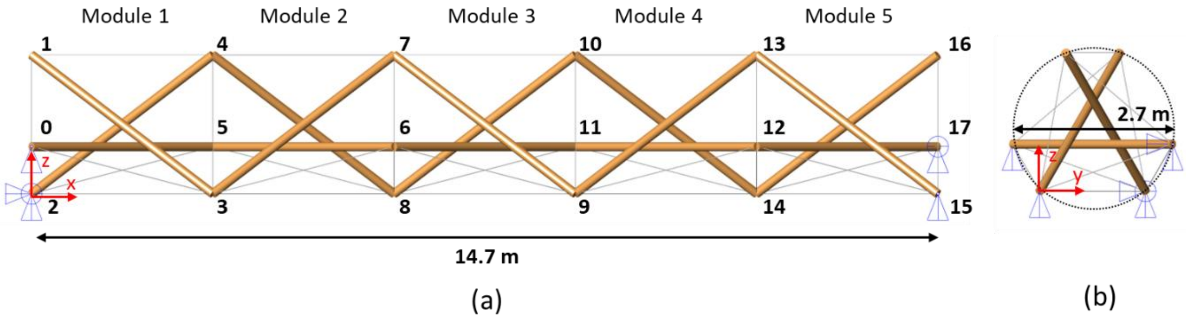

Fig. 10. Bamboo structure: (a) Front view and (b) side view.

Table 2. Materials and cross sections properties.

Elements	E [MPa]	f_y [MPa]	Diameter (mm)	Thickness (mm)	L_0 (mm)
Struts	6000	75	145	15	3928
Base cables	58000	700	10	/	2293
Top longitudinal cables	58000	700	10	/	3071
Bottom longitudinal cables with turnbuckles	60000	700	10	/	3071
Additional cables	58000	700	10	/	3408

The structure was prestressed and then loaded vertically (downwards) at nodes 7 and 10 in successive steps, as detailed in Table 3. For each step 1.0, 1.1, 1.2, and 1.3, prestress was introduced by shortening the bottom transverse cables: modules 1 (C2-5, C0-3) and 5 (C2-15, C14-17), then in modules 2 (C3-6, C5-8) and 4 (C11-14, C9-12), and finally in module 3 (C6-9, C8-11). Measurements carried out on some of the bamboos showed that the average maximum imperfection is $e_0/L_0 = 1/250$.

Table 3. Prestressing and loading protocol, with bold values indicating modifications compared to the previous prestressing or loading step.

Loading stage	Shortening of cables in modules 1 and 5 (mm)	Shortening of cables in modules 2 and 4 (mm)	Shortening of cables in module 3 (mm)	Load/node applied on nodes 7 and 10 (kN)
1.0 Initial configuration	7	13.3	17.3	/
1.1 Prestressing	**14**	**26.7**	**34.7**	/
1.2 Prestressing	**21**	**40**	**52**	/
1.3 Prestressing	**28**	**53.3**	**69.3**	/
2.1 Loading 5 kN	28	53.3	69.3	**2.5**
2.2 Loading 10 kN	28	53.3	69.3	**5**
2.3 Loading 15 kN	28	53.3	69.3	**7.5**

Fig. 11 compares the internal axial forces calculated by Muscle for the five struts and cables most affected by the presence of a geometrical imperfection, taken as $e_0/L_0 = 1/250$ for all struts, with respect to the case where perfectly straight struts are considered (i.e., $e_0 = 0$). It can be observed that:

- Force redistribution due to initial geometrical imperfection is non-negligible, becoming more significant at higher loads and proportionally more important for cables than for struts.
- All members, except for one strut and one cable, exhibit a reduction in their internal forces, attributable to the distribution of deformations between axial and bending components in imperfect structs.
- The strut exhibiting the largest relative difference in axial force due to the geometrical imperfection, $(N_{e_0=L_0/250} - N_{e_0=0})/N_{e_0=0}$, is strut S7-9 (Fig. 11(c)), reaching 11 % before the application of the external loads (i.e., at the end of step 1.3) and 21 % after external loading (i.e., at the end of step 2.3). This variation is substantial, particularly considering that S7-9 is one of the struts carrying a larger absolute axial force (Fig. 11(a)).

- The cable with the largest relative difference in axial load is C7-10, which reaches 13% before the application of external loads (i.e., at the end of step 1.3) and 99% after loading (i.e., at the end of step 2.3). This significant reduction can be attributed to near-complete relaxation of cable C7-10 due to the imperfection.
- The analysis of the nodal displacements (not shown herein) reveals that they are only slightly affected by geometric imperfections (less than 1%), despite the clear reduction in internal forces, which can be attributed to the significant prestressing and the structural redundancy provided by additional cables.

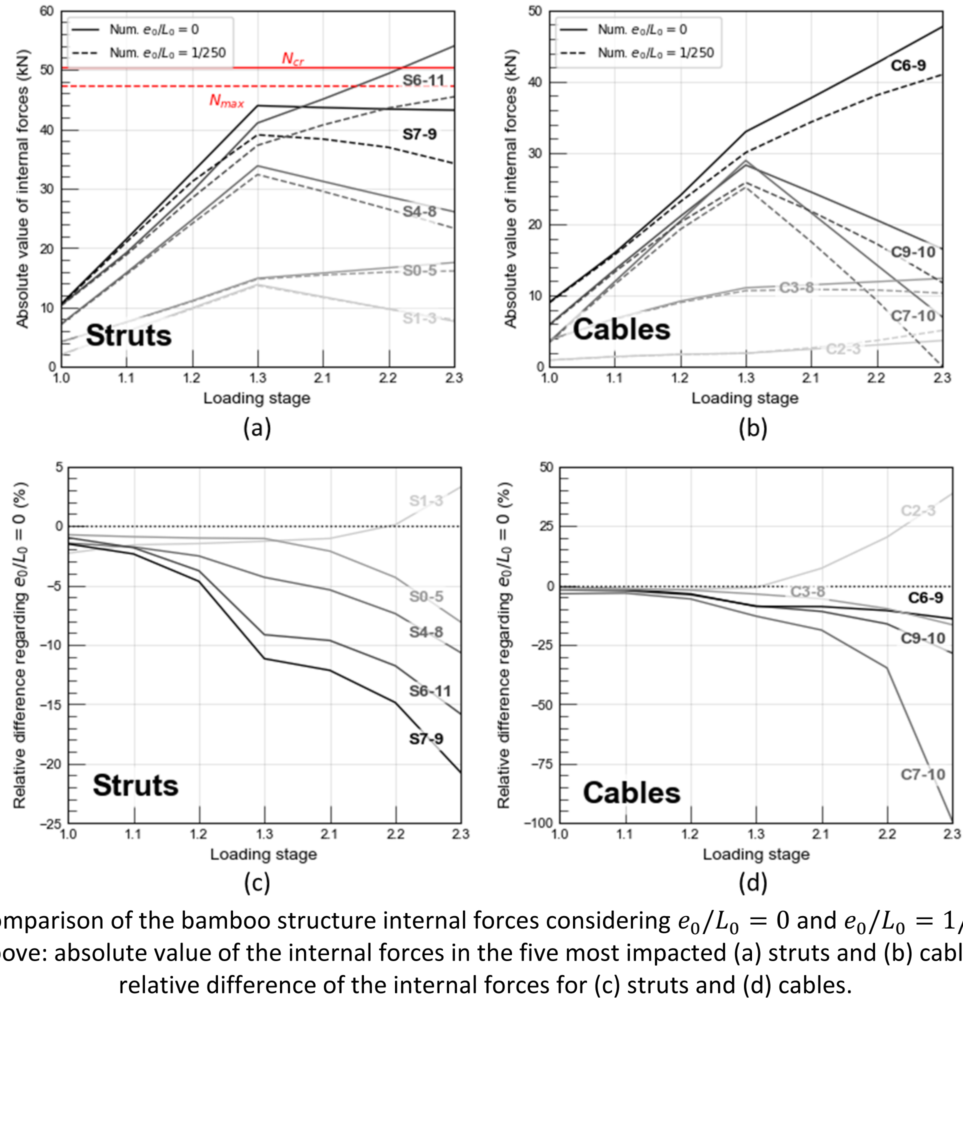

Fig. 11. Comparison of the bamboo structure internal forces considering $e_0/L_0 = 0$ and $e_0/L_0 = 1/250$ for all struts. Above: absolute value of the internal forces in the five most impacted (a) struts and (b) cables. Below: relative difference of the internal forces for (c) struts and (d) cables.

Fig. 12 is a variant of Fig. 11, corresponding to the particular case where all the struts are perfectly straight except for strut S7-9, which has an initial imperfection of $e_0/L_0 = 1/100$, i.e. slightly larger than in the preceding case where all struts had $e_0/L_0 = 1/250$.

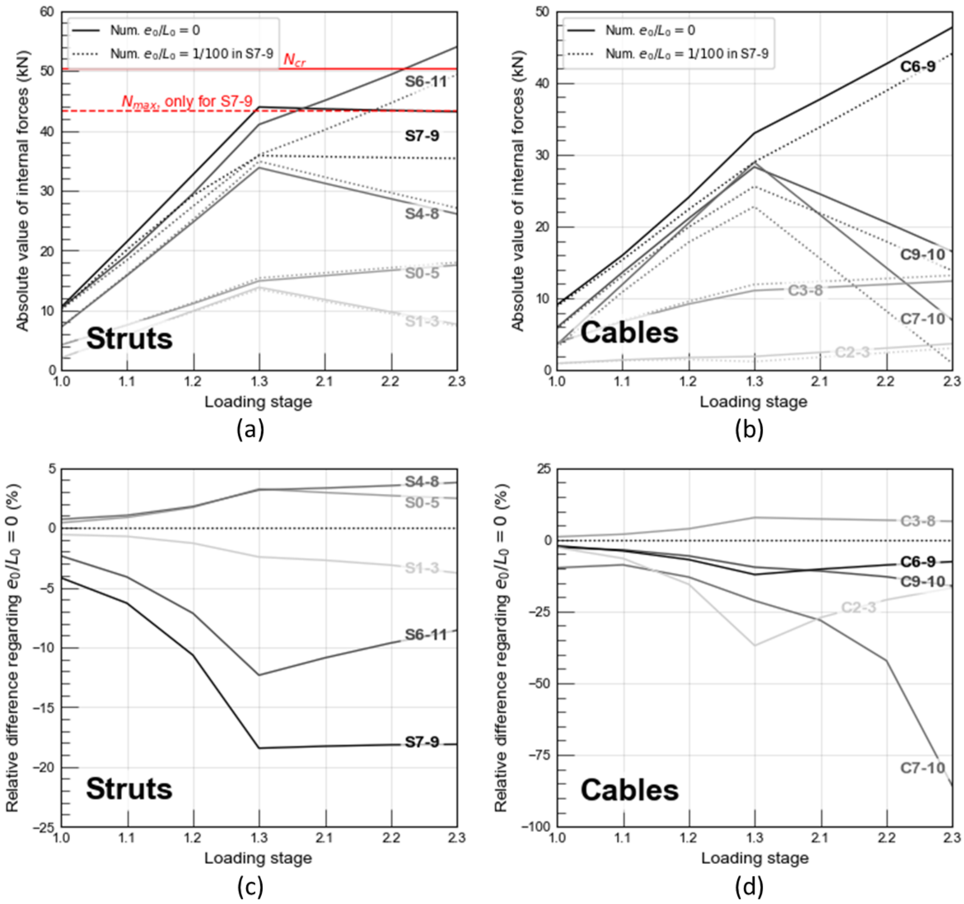

Fig. 12. Comparison of the bamboo structure internal forces considering $e_0/L_0 = 0$ and $e_0/L_0 = 1/100$ for strut S7-9 alone. Above: absolute value of the internal forces in the five most impacted (a) struts and (b) cables. Below: relative difference of the internal forces for (c) struts and (d) cables.

The following observations can be made from Fig. 12:

- Although only one strut is imperfect, the redistribution of internal forces affects the entire structure in a non-negligible manner.
- Similarly to the previous case, at the end of step 2.3 the imperfection leads to a complete relaxation of cable C7-10.
- The relative difference in axial force for the imperfect strut S7-9 due to the imperfection, $(N_{e_0/L_0=1/100} - N_{e_0/L_0=0})/N_{e_0/L_0=0}$, is equal to 19 % before application of the external loads (end of step 1.3) and 19 % after (end of step 2.3).
- If a less loaded strut (e.g., S1–3) had been considered imperfect (instead of S7–9), the overall impact would have been minor, as struts with low axial load do not experience significant stiffness reduction.

A geometrically nonlinear, beam-based DR formulation is currently under development in Muscle by the authors to further validate and benchmark the proposed approach in terms of both accuracy and computational efficiency. This formulation will also account for parasitic bending moments within the assemblies, a potential source of discrepancies between numerical predictions and experimental results that cannot be captured using a truss-based DR model.

CONCLUSIONS

Tensegrity structures combine at least three characteristics that engineers generally tend to avoid: they are often unstable at first order, they are not very rigid because they are made up of a large number of cables, and they require generalized prestressing, which can also have an impact on their self-weight. In addition to these three main characteristics, other phenomena related to connections, prestressing devices, and the struts and cables themselves exist, whose influence remains poorly understood. Among these, the authors, drawing on their experience in building and testing two large prototypes in their laboratory, have demonstrated that parasitic bending of the struts due to their geometric imperfections (i.e., out-of-straightness) can lead to a redistribution and modification of internal forces compared to values calculated using a model based on their initial stiffness L_0/EA. Some cables may even relax completely as a result. This limitation affects all current tensegrity calculation software, making them insufficiently reliable. with the same was true for the Muscle open-source software developed by the authors, which, prior to the research presented in this article, was unable to account for this phenomenon.

Taking this phenomenon into account purely through numerical means is very cumbersome, as subdividing each strut into a refined mesh of geometrically nonlinear beams greatly increases both computation time and code complexity. The authors have therefore chosen to develop a new analytical expression for the axial stiffness of struts, which shows that it depends on three dimensionless numbers alone: N/N_{cr}, e_0/L_0 and λ. These developments revisit the phenomenon of buckling, and the comparison of the results from this analytical relationship with those from two numerical nonlinear models as well as Eurocode 9 confirms its validity and supports its integration into a structural analysis code. The research has shown that, even for common eccentricities of $e_0/L_0 = 1/300$, the stiffness of a bar can decrease by 25% for a compression force equal to only half the critical force N_{cr}. It was also showed that the assumption of a sinusoidal initial shape for the struts is a conservative approach for design.

The developed analytical expression was then integrated in an iterative procedure to improve the Muscle numerical code, which now allows geometrical imperfections to be considered, making Muscle one of the most accurate tools for the analysis of tensegrity structures.

Using the improved Muscle code, two structures were calculated for a range of e_0/L_0 values. The sensitivity analysis applied to the aluminium simplex revealed an influence of the geometric imperfection in the struts on the internal force distribution. For the larger structure made up of five simplexes, some struts show a 21% decrease in internal forces for reasonable eccentricities equal to $e_0/L_0 = 1/250$, while the most impacted cables even relax completely.

The main overall conclusion of this investigation is that the geometric imperfection or out-of-straightness of struts cannot be ignored in the analysis of tensegrity structures, as it can lead to unforeseen behaviour or even collapse.

DATA AVAILABILITY STATEMENT:

Some data, models, or code that support the findings of this study are available from the corresponding author upon reasonable request. Some data, models, or code generated or used during the study are available in a repository online: Muscle GitHub: https://github.com/JonasFeron/Muscle.

ACKNOWLEDGEMENTS:

The authors would like to thank the French Community of Belgium – FSR program for the financial support. They also thank Jonas Feron for his contributions to the development of Muscle and for publishing it on GitHub and Food4Rhino.

NOTATION LIST:

The following symbols are used in this paper;

A (mm²) = strut cross-sectional area;

E (N/mm²) = strut Young's modulus;

e (mm) = strut deflection;

e_0(mm) = strut initial geometric imperfection;

f_y (MPa)= strut yield strength;

I (mm⁴) = cross section moment of inertia;

K (N/mm) = axial stiffness of a perfectly straight strut;

K_{red} (N/mm) = reduced equivalent axial stiffness of a strut with initial geometric imperfection;

L (mm) = chord length between the two supports of a strut for a given axial load;

L_0 (mm) = initial chord length between the two supports of a strut;

L_{bow} (mm) = bow length of a strut with imperfection, for a given axial load;

$L_{bow,0}$ (mm) = initial bow length of a strut with imperfection;

N (N) = axial load in the strut;

N_{cr}(N) = $\pi^2 EI/L_0^2$ = Euler critical load;

$N_{e_0/L_0=1/100}$ (N) = axial load in the strut with initial imperfection amplitude of $e_0/L_0 = 1/100$

$N_{e_0/L_0=0}$ (N) = axial load in the strut with initial imperfection amplitude of $e_0/L_0 = 0$

N_{max} (N) = axial force at first yielding of the strut;

W_{el} (mm³) = elastic section modulus;

λ (dimensionless) = $L_0\sqrt{A/I}$ = slenderness ratio;

λ_{rel} (dimensionless) = $\sqrt{Af_y/N_{cr}}$ = relative slenderness ratio;

REFERENCES:

Barnes, M. R. 1999. “Form Finding and Analysis of Tension Structures by Dynamic Relaxation.” International Journal of Space Structures, 14 (2): 89–104. https://doi.org/10.1260/0266351991494722.

Barnes, M. R., S. Adriaenssens, and M. Krupka. 2013. “A novel torsion/bending element for dynamic relaxation modeling.” Computers & Structures, 119: 60–67. https://doi.org/10.1016/j.compstruc.2012.12.027.

Bel Hadj Ali, N., L. Rhode-Barbarigos, and I. F. C. Smith. 2011. “Analysis of clustered tensegrity structures using a modified dynamic relaxation algorithm.” International Journal of Solids and Structures, 48 (5): 637–647. https://doi.org/10.1016/j.ijsolstr.2010.10.029.

Cai, J., X. Wang, R. Yang, and J. Feng. 2018. “Mechanical behavior of tensegrity structures with High-mode imperfections.” *Mechanics Research Communications*, 94: 58–63. https://doi.org/10.1016/j.mechrescom.2018.09.006.

Cai, J., R. Yang, X. Wang, and J. Feng. 2019. “Effect of initial imperfections of struts on the mechanical behavior of tensegrity structures.” *Composite Structures*, 207: 871–876. https://doi.org/10.1016/j.compstruct.2018.09.018.

CEN (European Committee for Standardization). 2005. “Eurocode 3: Design of steel structures - Part 1-1: General rules and rules for buildings.”

CEN (European Committee for Standardization). 2007. “Eurocode 9: Design of aluminum structures - Part 1-1 : General structural rules.”

Feron, J. 2025. “Muscle.” Accessed May 1 2025. https://github.com/JonasFeron/Muscle

Feron, J., A. Bertholet, and P. Latteur. 2022. “Replication Data for: Experimental testing of a tensegrity simplex: self-stress implementation and static loading.” Open Data @ UCLouvain. https://doi.org/10.14428/DVN/CDLVFV.

Feron, J., L. Boucher, V. Denoël, and P. Latteur. 2019. “Optimization of Footbridges Composed of Prismatic Tensegrity Modules.” *J. Bridge Eng.*, 24 (12): 04019112. https://doi.org/10.1061/(ASCE)BE.1943-5592.0001438.

Feron, J., and P. Latteur. 2023. “Implementation and propagation of prestress forces in pin-jointed and tensegrity structures.” *Engineering Structures*, 289: 116152. https://doi.org/10.1016/j.engstruct.2023.116152.

Feron, J., B. Payen, J. Almeida, and P. Latteur. 2024. “MUSCLE: a new open-source Grasshopper plug-in for the interactive design of tensegrity structures.” http://hdl.handle.net/2078.1/291034.

Feron, J., L. Rhode-Barbarigos, and P. Latteur. 2023. “Experimental Testing of a Tensegrity Simplex: Self-Stress Implementation and Static Loading.” *J. Struct. Eng.*, 149 (7): 04023073. https://doi.org/10.1061/JSENDH.STENG-11517.

Jeppe Jönsson, J. Jönsson, Tudor-Cristian Stan, and T.-C. Stan. 2017. “European column buckling curves and finite element modelling including high strength steels.” *Journal of Constructional Steel Research*, 128: 136–151. https://doi.org/10.1016/j.jcsr.2016.08.013.

Kucukler, M., L. Gardner, and L. Macorini. 2014. “A stiffness reduction method for the in-plane design of structural steel elements.” *Engineering Structures*, 73: 72–84. https://doi.org/10.1016/j.engstruct.2014.05.001.

Labrouche, V., and T. Houriez. 2023. “Etude expérimentale d’une structure en tenségrité.” MA thesis. UCLouvain. http://hdl.handle.net/2078.1/thesis:43356.

Latteur, P., J. Feron, and V. Denoel. 2017. “A design methodology for lattice and tensegrity structures based on a stiffness and volume optimization algorithm using morphological indicators.” *International Journal of Space Structures*, 32 (3–4): 226–243. https://doi.org/10.1177/0266351117746267.

Maquoi, R., and J. Rondal. 1978. “Analytical Formulation of the New European Buckling Curves.”

McNeel, R. 2025. “Rhinoceros 3D (Version 7.0.).” Robert McNeel & Associates.

Micheletti, A., and P. Podio-Guidugli. 2022. “Seventy years of tensegrities (and counting).” *Arch Appl Mech*, 92 (9): 2525–2548. https://doi.org/10.1007/s00419-022-02192-4.

Motro, R. 2003. “Tensegrity: Structural systems for the future.” *Kogan Page Science*. https://doi.org/10.1016/B978-1-903996-37-9.X5028-8.

Pellegrino, S. 1993. “Structural computations with the singular value decomposition of the equilibrium matrix.” *International Journal of Solids and Structures*, 30 (21): 3025–3035. https://doi.org/10.1016/0020-7683(93)90210-X.

Preisinger, C. 2013. “Linking Structure and Parametric Geometry.” *Architectural Design*, (83): 110–113. https://doi.org/DOI: 10.1002/ad.1564.

Rhode-Barbarigos, L., C. Schulin, N. B. H. Ali, R. Motro, and I. F. C. Smith. 2012. “Mechanism-Based Approach for the Deployment of a Tensegrity-Ring Module.” *J. Struct. Eng.*, 138 (4): 539–548. https://doi.org/10.1061/(ASCE)ST.1943-541X.0000491.

Rutkiewicz, A., and L. Małyszko. 2024. “Experimental and numerical static tests of tensegrity triplex modules.” *Bulletin of the Polish Academy of Sciences Technical Sciences*, 151674–151674. https://doi.org/10.24425/bpasts.2024.151674.

Saufnay, L., J.-P. Jaspart, and J.-F. Demonceau. 2024. “Improvement of the prediction of the flexural buckling resistance of hot-rolled mild and high-strength steel members.” *Engineering Structures*, 315: 118460. https://doi.org/10.1016/j.engstruct.2024.118460.

Seismosoft. 2024. “SeismoStruct.”

Shekastehband, B., K. Abedi, and N. Dianat. 2013. “Experimental and numerical study on the self-stress design of tensegrity systems.” *Meccanica*, 48 (10): 2367–2389. https://doi.org/10.1007/s11012-013-9754-3.

Somodi, B., E. Bärnkopf, and B. Kövesdi. 2023. “Applicable equivalent bow imperfections in GMNIA for Eurocode buckling curves – SHS, RHS and welded box sections.” *Journal of Constructional Steel Research*, 204: 107860. https://doi.org/10.1016/j.jcsr.2023.107860.

UCLouvain GCE. 2020. "The Snake Bridge". Accessed April 18, 2025. https://www.youtube.com/watch?v=mqV6k-HpDqs.

UCLouvain GCE. 2023. "Deux étudiants ingénieurs explorent les mystères de la tenségrité à l’UCLouvain". Accessed March 27, 2025 . https://www.youtube.com/watch?v=cJN3jXL6NQk&t=30s.

Wang, Y., X. Xu, and Y. Luo. 2021. “Form-finding of tensegrity structures via rank minimization of force density matrix.” *Engineering Structures*, 227: 111419. https://doi.org/10.1016/j.engstruct.2020.111419.

Xu, X., Y. Wang, Y. Luo, and D. Hu. 2018. “Topology Optimization of Tensegrity Structures Considering Buckling Constraints.” *J. Struct. Eng.*, 144 (10): 04018173. https://doi.org/10.1061/(ASCE)ST.1943-541X.0002156.

Zhang, J. Y., and M. Ohsaki. 2006. “Adaptive force density method for form-finding problem of tensegrity structures.” *International Journal of Solids and Structures*, 43 (18–19): 5658–5673. https://doi.org/10.1016/j.ijsolstr.2005.10.011.